EVALUATION OF THE EFFECTS OF PRINTING PARAMETERS AND NEW BIOINK COMPOSITION ON GREEN BIOPRINTED CONSTRUCTS

A Thesis

by

LAURA RENEE JERPSETH

Submitted to the Graduate and Professional School of
Texas A&M University
in partial fulfillment of the requirements for the degree of

MASTER OF SCIENCE

Chair of Committee,	Hongmin Qin
Committee Members,	Zhijian Pei
	Deborah Bell-Pedersen
Head of Department,	Alex Keene

December 2021

Major Subject: Microbiology

ABSTRACT

Bioprinting is an additive manufacturing process capable of fabricating bioprinted constructs containing cells via layer-by-layer deposition of bioink. Bioink contains the cells using during bioprinting, and may contain additional materials to promote cell adhesion, cell viability, structural integrity, and/or shape fidelity of bioprinted constructs. While bioprinting using mammalian cells has been extensively studied, less research has been conducted regarding bioprinting using photosynthetic cells, also known as green bioprinting. Potential benefits of green bioprinting include production and easy harvesting of metabolites for use in the pharmaceutical, cosmetic, and food industries. Constructs fabricated using green bioprinting have also been shown to remove metal from water, and green bioprinted constructs are capable of providing oxygen to mammalian cells in order to supplement tissue engineering research.

Despite potential benefits, more research is required to determine the optimal printing parameters for green bioprinting. In order to be functional, bioprinted constructs must have high cell viability post bioprinting. Research was conducted to test the effects of variable extrusion pressures and needle diameters on *Chlamydomonas reinhardtii* algae cell viability in green bioprinted constructs. It was determined that increasing extrusion pressure and decreasing needle diameter decreased the cell viability in green bioprinted constructs.

Additionally, in currently published literature, only two bioinks have been used for green bioprinting applications. These bioinks, alginate:methylcellulose and alginate:agarose:methylcellulose, promote high photosynthetic cell viability. However, the bioinks do not have sufficient physical properties to bioprint constructs with high shape fidelity. A new bioink, alginate:methylcellulose:GelMA, was synthesized to improve the shape fidelity of green

bioprinted constructs while maintaining high cell viability. Constructs bioprinted with alginate:methylcellulose:GelMA bioink were tested for *Chlamydomonas reinhardtii* algae cell viability and shape fidelity of the bioprinted constructs. Rheological analysis was also performed of a sample of unprinted alginate:methylcellulose:GelMA bioink to determine if the viscosity of the bioink is suitable for use with bioprinting. It was determined that alginate:methylcellulose:GelMA bioink has suitable viscosity, and can be used to bioprint green constructs with high cell viability and shape fidelity.

CONTRIBUTORS AND FUNDING SOURCES

Contributors

This work was supervised by a thesis committee consisting of Professor Hongmin Qin and Professor Deborah Bell-Pedersen of the Department of Biology and Professor Zhijian Pei of the Department of Industrial & Systems Engineering.

All research and experimentation described in this thesis were conducted as a collaboration between the laboratories of Professor Hongmin Qin and Professor Zhijian Pei. Ketan Thakare, an Industrial & Systems Engineering PhD student under the advisement of Dr. Pei, assisted in all experimentation. Ketan Thakare designed the CAD models used during bioprinting, controlled the bioprinter during experimentation, and assisted with data collection and analysis. During experimentation, the author of this thesis cultivated required cells, synthesized bioink, and gathered cell viability data.

Funding Sources

Graduate study was supported by a Teaching Assistantship from the Biology Department at Texas A&M University.

NOMENCLATURE

CAD	Computer aided design
STL	StereoLithography
TAP	Tris-acetate-phosphate
GelMA	Gelatin methacryloyl
PEG	Polyethylene glycol
PEGDA	Polyethylene glycol diacrylate
ANOVA	Analysis of variance

TABLE OF CONTENTS

LIST OF FIGURES

LIST OF TABLES

1. INTRODUCTION

1.1. Bioprinting Applications and Techniques

Bioprinting technology was initially developed with the objective of mitigating limitations of 2D cell cultures and animal models in tissue research [1]. Cells in 2D cultures lack the complex physiological morphology present in actual *in vivo* environments [2, 3]. As a result, 2D cell cultures cannot adequately model cell signaling, nutrient and oxygen gradients, and tissue responses to external stimuli [4], and these limitations have hindered drug research [5]. Animal models are expensive and do not precisely represent human physiology [6]. Bioprinting is capable of fabricating 3D cell cultures with more precise cell distributions than previous 3D cell culturing techniques [7]. Because bioprinted constructs more closely resemble native tissue environments, bioprinting has applications in research involving drug testing [8], organ fabrication [9], and disease modeling [10].

There are currently three main bioprinting techniques, each with unique advantages and disadvantages. These techniques include extrusion-based, inkjet-based, and laser-assisted bioprinting [11]. For each bioprinting technique, the bioink can be precisely deposited along the x-axis, y-axis, and z-axis to form bioprinted constructs with precise dimensions. Before bioprinting can occur, computer software must be used to generate a 3D model of the construct to be fabricated by the bioprinter. To form the 3D model, computer aided design (CAD) software in the StereoLithography (STL) file format is often used [12]. The STL file must then be converted to G-code in order to be compatible with the bioprinter [12].

The extrusion-based bioprinting technique is illustrated in Figure 1. Bioink is dispensed from the extrusion nozzle using pressure generated by either compressed air or a mechanical screw.

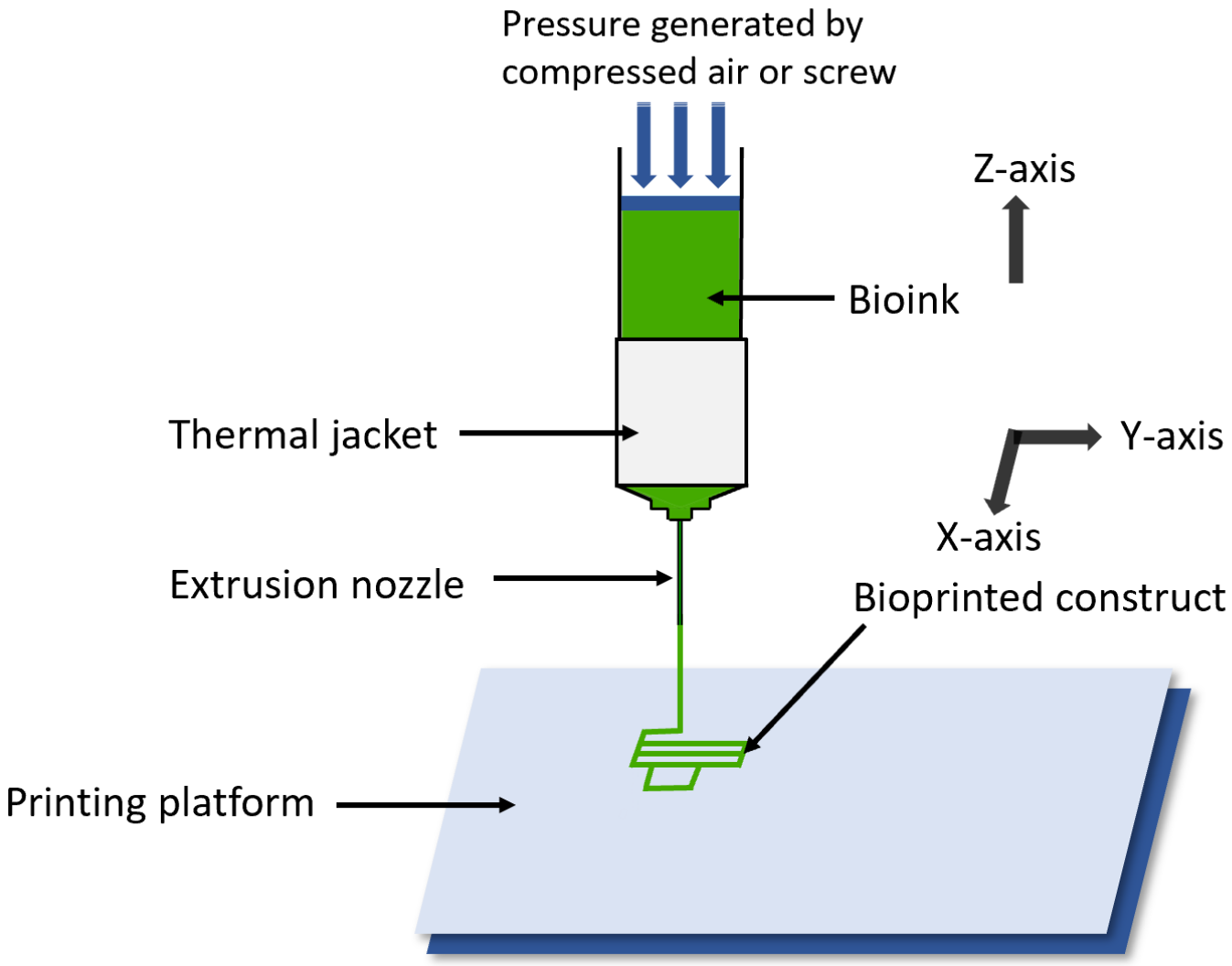

Figure 1. Illustration of extrusion-based bioprinting.

The bioprinted construct is fabricated on top of the printing platform. The thermal jacket of the bioprinter can be used to control the temperature of the bioink. Advantages of extrusion-based bioprinting include compatibility with bioinks with a high cell concentration, and capability of bioprinting bioinks with a wide range of viscosities [13]. Extrusion-based bioprinters are also capable of bioprinting porous constructs [14], which allows vascularized constructs to be bioprinted [15]. However, in order to be compatible with extrusion-based bioprinting, bioinks must exhibit shear-thinning behavior [16]. The viscosity of matter with shear-thinning behavior decreases as shear stress increases [17]. Conversely, as shear stress decreases, the viscosity of matter with shear-thinning behavior increases [17]. Extrusion-based bioprinting exposes bioink to mechanical stress as bioink is extruded from the extrusion nozzle [11]. Shear-thinning behavior is necessary because it allows bioink to be smoothly extruded from the extrusion nozzle during bioprinting, and the shape of bioprinted constructs is maintained post bioprinting [18]. Another disadvantage of extrusion-based bioprinting is decreased resolution of bioprinted constructs compared to other techniques [19, 20].

An illustration of inkjet bioprinting is shown in Figure 2. A thermal or piezoelectric actuator creates droplets of bioink that are ejected from the tubular column. The actuator controls the size of bioink droplets, and the droplets form the bioprinted construct on the printing platform. Advantages of inkjet bioprinting include high resolution and high cell viability of bioprinted constructs [21]. Disadvantages of inkjet bioprinting include the inability to bioprint high viscosity bioinks, and inability to bioprint bioinks with a high cell concentration [11].

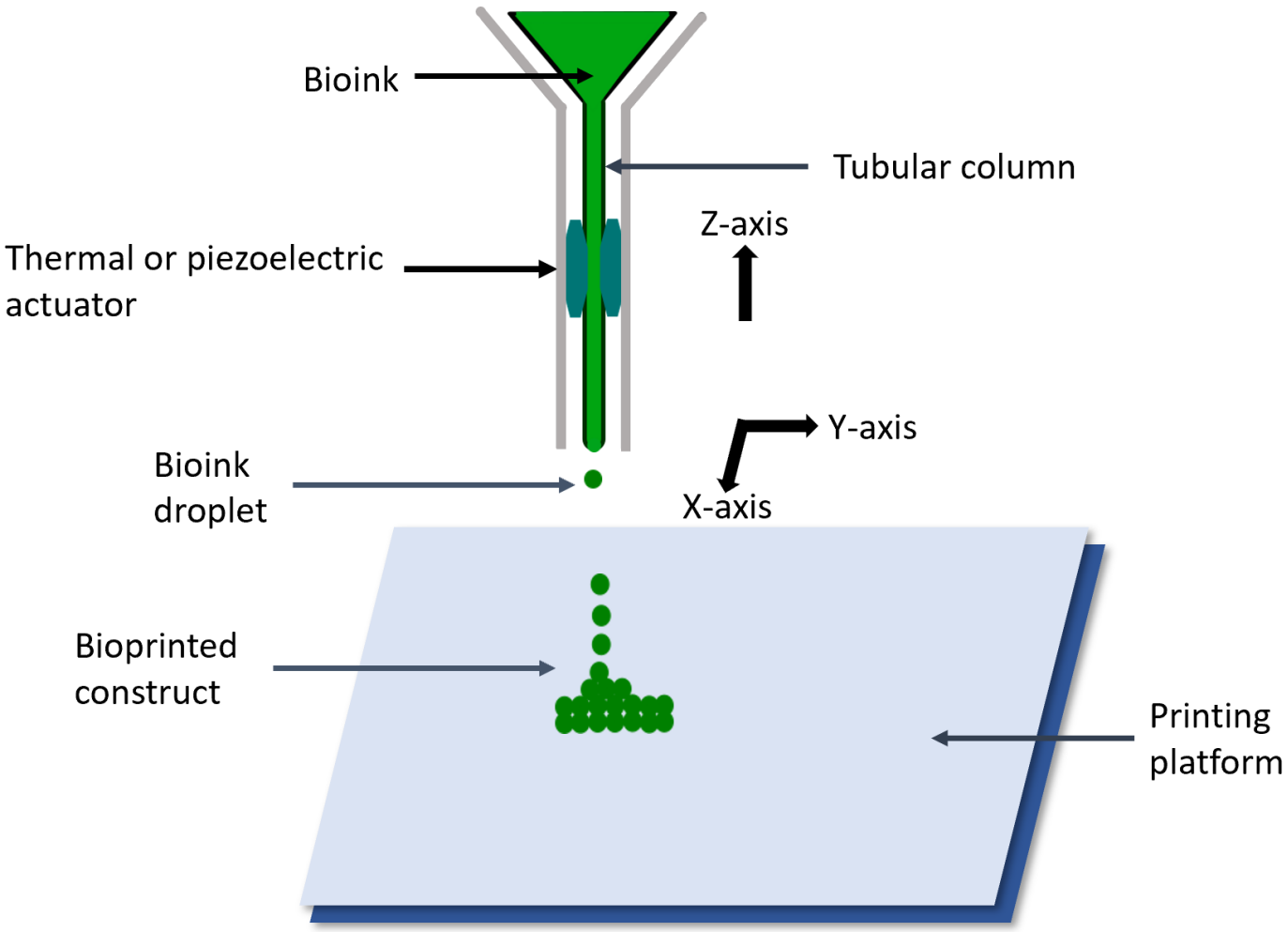

Figure 2. Illustration of inkjet bioprinting.

An illustration of laser-assisted bioprinting is shown in Figure 3. A laser is passed through a focusing lens onto a donor layer capable of absorbing energy, such as titanium film [22], and a layer of bioink is positioned below the energy absorbing layer. When the laser comes into contact with the energy absorbing material of the donor layer, a portion of the material is vaporized and a droplet of bioink is ejected from the bioprinter. The droplets of bioink form a bioprinted construct on the printing platform. The cells in the bioink are not exposed to mechanical stress, and the laser does not come into direct contact with the bioink. For these reasons, laser-assisted bioprinting bioprints constructs with high cell viability [23, 24]. Additional advantages of laser-assisted bioprinting include high printing resolution [25, 26] and the ability to print high-viscosity bioinks [27 – 29]. However, laser-assisted bioprinting is expensive and difficult to use [11], which are disadvantages compared to other bioprinting techniques.

1.2. Green Bioprinting

A subset of bioprinting known as green bioprinting uses photosynthetic cells instead of mammalian cells in bioink. Photosynthetic cells in green bioprinted constructs are immobilized. Previous research has revealed that immobilized photosynthetic cells grow to a higher cell density than cells suspended in liquid medium [30, 31], and produce more metabolites [32]. These conditions are ideal for production of commercially beneficial metabolites produced by photosynthetic cells. Examples of commercially beneficial metabolites include phenols used as flavoring agents [33], terpenoids used as odorants [33], and sugar alcohols used as artificial sweeteners [34]. Traditional photosynthetic cell immobilization methods, such as immobilization in alginate beads [35], do not allow for precise positioning of cells or formation of complex constructs [30]. Alginate beads also degrade over time in liquid [36]. Green bioprinting overcomes the limitations of traditional immobilization methods.

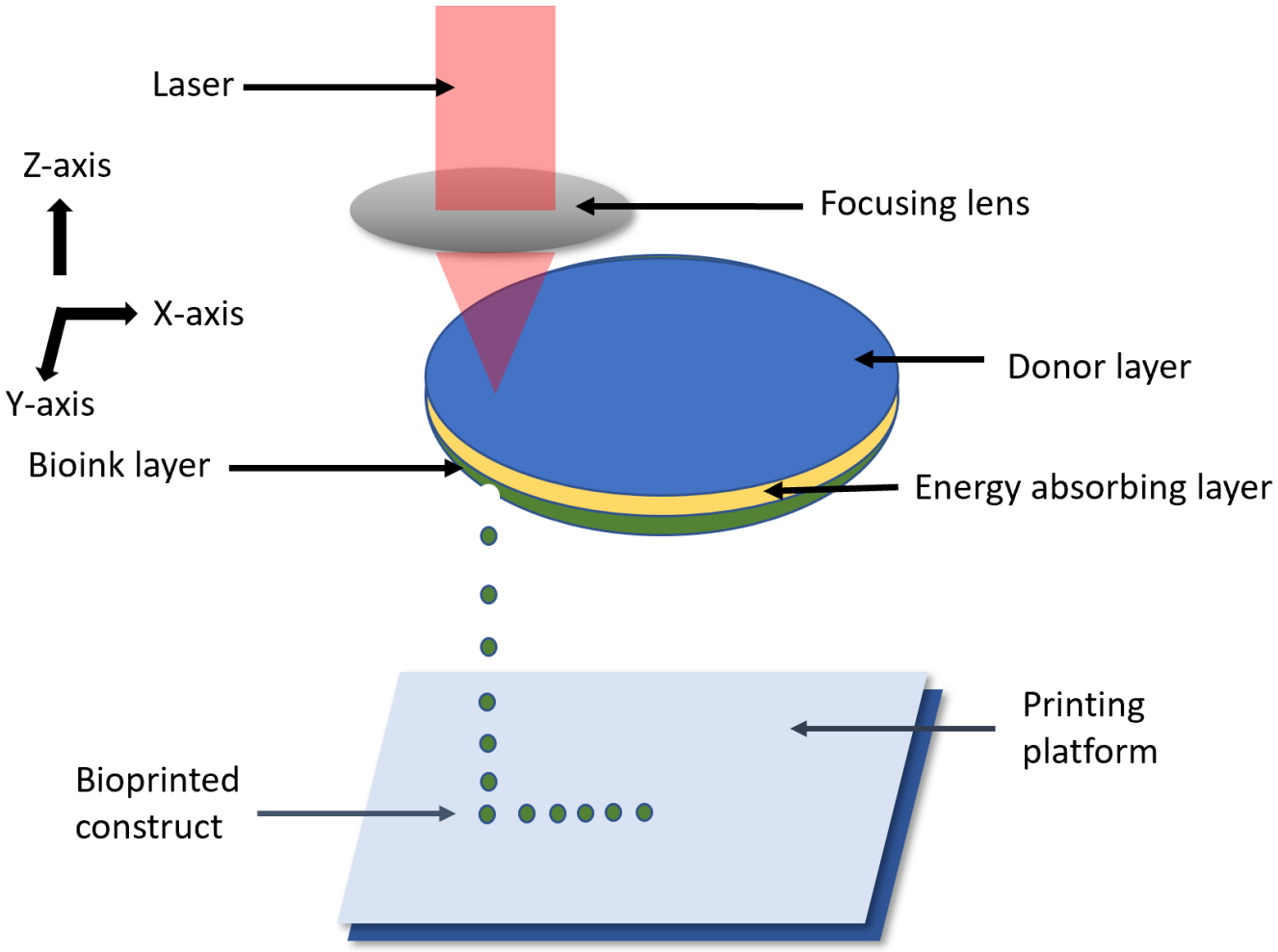

Figure 3. Illustration of laser-assisted bioprinting.

Green bioprinting fabricates constructs with complex geometries [30], cells can be evenly distributed inside green bioprinted constructs [37], and green bioprinted constructs are resistant to dissolving [38].

Lode et al. used green bioprinting to deliver oxygen to bioprinted bone cells [30]. *Chlamydomonas reinhardtii* algae cells in alginate:methylcellulose bioink were bioprinted in a grid pattern adjacent to bone cells. Analyses performed 12 days post bioprinting indicated that both the algae and bone cells were living, and the oxygen production rate increased five-fold between the day 1 and day 12 post bioprinting. The results of this research show promise for the use of green bioprinting in tissue engineering research. Green bioprinting may be used concurrently with mammalian cell bioprinting to provide necessary oxygen to the mammalian cells.

Krujatz et al. studied the cell viability and growth between algae cells immbolized in green bioprinted constructs and algae cells suspended in liquid tris-acetate-phosphate (TAP) medium [31]. Two species of algae cells were studied, *Chlamydomonas reinhardtii* and *Chlorella sorokiniana*. Additionally, temperature and length of light/dark cycles were varied for both test conditions. It was concluded that algae in green bioprinted constructs maintained a more stable growth rate in suboptimal temperatures and light cycles than algae suspended in TAP.

Seidel et al. formulated a new bioink composition, alginate:agarose:methylcellulose, for use in green bioprinting [37]. The bioink was tested for shear-thinning behavior to evaluate its compatibility with extrusion-based bioprinting. The bioink exhibited shear-thinning behavior and was therefore compatible with extrusion-based bioprinting. Basil cells were added to alginate:agarose:methylcellulose, and constructs in the shape of a grid were bioprinted with the bioink. The bioprinted constructs were evaluated up to 21 days post bioprinting. The shape fidelity

of the bioprinted constructs was determined by measuring the width of the strands in the constructs. Shape fidelity describes how closely a bioprinted construct matches the CAD model used during bioprinting. Cell viability was also measured in the bioprinted constructs by performing live/dead staining. The study concluded that alginate:agarose:methylcellulose has sufficient shear-thinning, shape fidelity, and cell viability to be successfully used as a bioink for green bioprinting.

Thakare et al. fabricated green bioprinted constructs that were used as filters to remove copper from water [38]. Alginate:methylcellulose containing *Chlamydomonas reinhardtii* algae cells was used as the bioink during bioprinting. After 2 hours of contact with the green bioprinted filters, the copper concentration in the water was below 0.001 ppm. The green bioprinted filters containing algae were also shown to be more efficient at removing copper from water than alginate:methylcellulose filters without algae.

1.3. Bioink Compositions and Crosslinking Mechanisms

Bioink is the material deposited by bioprinters to fabricate bioprinted constructs. Bioinks must contain cells [39], and frequently also contain polymers capable of absorbing and retaining water, known as hydrogels [40]. Bioinks containing hydrogels are permeable, which allows diffusion of atmospheric gases and nutrients through bioprinted constructs [40]. The permeability of bioprinted constructs also allows cells to be evenly distributed throughout the construct [41]. A variety of hydrogels are currently used in bioink synthesis, and hydrogels may be used to increase cell adhesion, cell viability, structural integrity, and/or shape fidelity of bioprinted constructs [39].

Different hydrogels have unique advantages and disadvantages, and hydrogels can be either naturally derived or synthetically derived [16]. Natural hydrogels that are derived from animals include collagen, fibrin, and gelatin. These hydrogels contain cell signaling molecules that

promote cell adhesion to the bioink [16], which promotes growth of mammalian cells in bioprinted constructs. Other natural hydrogels are derived from photosynthetic sources and include alginate, agarose, and cellulose. Although these hydrogels do not contain cell signaling molecules that are beneficial for mammalian cell bioprinting [42, 43], hydrogels derived from photosynthetic sources promote high cell viability and growth in green bioprinted constructs [30, 31, 37]. While naturally derived hydrogels promote high cell viability, the mechanical properties of these hydrogels are weak and do not promote strong structural integrity [44]. Bioprinted constructs must have high structural integrity in order to prevent the construct from collapsing [45]. Structural integrity is also necessary for bioprinted constructs to maintain high shape fidelity [37]. Because of this, bioinks with only naturally derived hydrogels may be limited in the complexity and size of constructs that can be bioprinted.

Synthetically derived hydrogels include gelatin methacryloyl methacryloyl (GelMA), Pluronic, and polyethylene glycol (PEG). These hydrogels do not contain signaling molecules [44], and the cell viability in constructs bioprinted with synthetically derived hydrogels is not as high as constructs bioprinted with naturally derived hydrogels [16]. However, synthetically derived hydrogels have high structural integrity, and have been used to bioprint complex structures for tissue engineering research [46].

Cell viability, structural integrity, and shape fidelity of bioprinted constructs are affected by crosslinking mechanisms in addition to bioink composition. Crosslinking forms bonds between the polymers of hydrogels in bioprinted constructs [47], and is necessary for constructs to maintain shape after being bioprinted [47]. Different hydrogels are compatible with different crosslinking mechanisms. Hydrogels made of polysaccharides, including alginate, are ionically crosslinkable [48]. Ionic crosslinking can be performed at room temperature and physiological pH, but ionically

crosslinked constructs have lower structural integrity than constructs crosslinked with other mechanisms [47]. Ionic crosslinking can also cause bioprinted constructs to swell and decrease shape fidelity [37].

Photo-crosslinking is a crosslinking mechanism compatible with photocurable hydrogels such as GelMA [49], Pluronic [50], and polyethylene glycol diacrylate (PEGDA) [51]. In order to perform photo-crosslinking, a photoinitiator must be added to photocurable hydrogel [47]. When light of a specific wavelength comes into contact with the photoinitiator, the photoinitiator dissociates and free radicals are formed which crosslink the bioprinted construct [47]. UV light is mostly commonly used for photo-crosslinking, although the use of UV light can damage cells in bioprinted constructs [47]. However, advantages of photo-crosslinking include high spatiotemporal control and the ability to crosslink constructs with high structural integrity and shape fidelity [47].

1.4. Aims

Despite the benefits of green bioprinting, it is currently unknown how variable printing parameters affect the cell viability in green bioprinted constructs. Extrusion-based bioprinting studies using mammalian cells have revealed that cell viability of mammalian cells decrease as extrusion pressure increases [52 – 54] or nozzle diameter decreases [53 – 55], likely due to an increase of shear stress. Additionally, different cell types exhibit different sensitivities to extrusion pressure and nozzle diameter during bioprinting [56]. Because photosynthetic cells have significantly different anatomy compared to mammilian cells, including presence of a cell wall, the effect of various extrusion pressure and nozzle diameter values on cell viability in green bioprinting warrants further research. The effects of extrusion pressure and nozzle diameter on the cell viability of alginate:methylcellulose bioink containing *Chlamydomonas reinhardtii* algae cells

were determined. Alginate:methylcellulose containing *Chlamydomonas reinhardtii* was used as the bioink because it is the bioink most frequently used for green bioprinting applications [30, 31, 38].

An additional aim is to synthesize a new bioink for use with green bioprinting. Currently, alginate:methylcellulose [30, 31, 38] and alginate:agarose:methylcellulose [37] are the only bioinks that have been successfully used for green bioprinting. Although these bioinks have high cell compatibility [Jia 2014], constructs of limited shape fidelity and structural integrity are bioprinted with these bioinks [44]. A new bioink, alginate:methylcellulose:GelMA, was synthesized in order to combine the advantages of naturally derived, ionically crosslinkable hydrogels (alginate and methylcellulose) with the advantages of synthetically derived, photo-crosslinkable hydrogel (GelMA). Alginate is intended to promote high cell viability and growth of the photosynthetic cells in the green bioprinted construct. Methylcellulose modifies the viscosity of the bioink [18] to ensure proper printability, and GelMA provides greater structural integrity, shape fidelity, and photo-crosslinking [49]. Alginate:methylcellulose:GelMA was evaluated for its shear thinning behavior to determine the compatibility of the bioink with extrusion-based bioprinting. Constructs bioprinted with alginate:methylcellulose:GelMA containing *Chlamydomonas reinhardtii* algae cells were evaluated for shape fidelity and cell viability to determine if the bioink can be successfully used for green bioprinting applications.

2. MATERIALS AND METHODS

2.1. Determining the Effects of Variable Extrusion Pressure and Nozzle Diameter on the Cell Viability of Green Bioprinted Constructs

2.1.1. Algae Preparation

Chlamydomonas reinhardtii algae strain cc125 cells was streaked off a solid TAP petri dish and added to a flask containing 100 milliliters of liquid TAP. To maintain sterile conditions, the addition was done in a biosafety cabinet (SterilGARD III Advance, Baker, USA). The algae cells used in this study were obtained from the Chlamydomonas Center (Chlamydomonas Resource Center, University of Minnesota). The TAP-algae solution was placed on a well-lit shaker (New Brunswick Scientific Co., Inc, USA) for 72 hours to allow the algae cells to grow. The shaker was run at 100 rpm and kept at 22 °C. On the day of bioprinting was performed, the algae cell concentration in the TAP-algae solution was measured using Auto T4 cell counter (Nexcelom, USA) according to the instructions from the cell counter manufacturer.

2.1.2. Alginate:methylcellulose Bioink Synthesis

Three grams of alginic acid sodium salt (Sigma-Aldrich, USA) were added to 100 milliliters of deionized water in a beaker. This alginate solution was stirred with a magnetic stir bar (Fisher Scientific, USA) at 900 rpm for five hours on a hot plate stirrer (Fisher Scientific, USA). The hot plate stirrer was then heated to 90°C, and six grams of methylcellulose powder (Sigma-Aldrich, USA) were added to the alginate solution to synthesize alginate:methylcellulose. The solution was stirred for an additional 30 minutes to ensure a homogenous distribution of the components. The alginate:methylcellulose solution was autoclaved (LG 250 Sterilizer, Steris, USA) for one minute at 121°C to achieve sterilization without burning the methylcellulose. After

the alginate:methylcellulose cooled to room temperature, TAP-algae solution was added to the alginate:methylcellulose. The addition of algae cells was performed by pipette in a biosafety cabinet to synthesize a bioink with a cell concentration 150,000 cells/milliliter.

2.1.3. Construct Design

The construct 3D model was designed using Fusion 360 software (Autodesk, USA). The construct model was disk-shaped with diameter of 15 millimeters and thickness of 1.5 millimeters. Fusion 360 software generated an STL file that was converted into a G-code file using SLICER software (SLICER.org, USA). This G-code file was then imported into Allevi bioprinter software (Allevi Inc, USA).

2.1.4. Bioprinting

Allevi 2 bioprinter (Allevi Inc, USA), an extrusion-based bioprinter, was used to bioprint the constructs. The alginate:methylcellulose bioink was loaded into an extrusion syringe, and the constructs were printed on microscope slides inside petri dishes. Bioprinting was performed inside a biosafety cabinet to maintain sterility. Post bioprinting, the constructs were submerged in 100 millimolar $CaCl_2$ solution for 4 minutes to achieve ionic crosslinking. After crosslinking, the $CaCl_2$ solution was removed from the petri dishes using Kimwipes (Kimtech, USA), and liquid TAP medium was added to the petri dishes to promote algae cell growth and prevent the bioprinted constructs from drying out. The petri dishes were placed under lightbulbs to promote additional algae cell growth.

2.1.5. Experimental Design

Two sets of one-factor-at-a-time experiments were conducted to investigate the effects of variable extrusion pressure and nozzle diameter values on cell viability. For the first set of

experiments, constructs were bioprinted by varying extrusion pressure values. The three levels of extrusion pressure were 3, 5, and 7 bar. Nozzle diameter was kept constant at 250 µm for the first set of experiments. For the second set of experiments, samples were bioprinted by varying nozzle diameter values. The three levels of nozzle diameter were 200, 250, and 400 µm. Extrusion pressure was kept constant at 4 bar. Three constructs were printed as replicates at each experimental condition for both sets of experiments.

2.1.6. Cell Viability Assessment

Cell viability was determined by measuring the cell growth in the bioprinted constructs. Confocal microscopy, FV1000 microscope (Olympus, Inc., USA), was used in this study to measure the cell concentration in the bioprinted constructs three days and six days post printing. The measurement procedure is described stepwise below:

Step 1: The average number of algae cells in an algae cell cluster, A, was estimated. In the green bioprinted constructs, algae cells grew in clusters instead of being evenly distributed. Images of five randomly chosen algae cell clusters on the sample surface were taken for each bioprinted construct. Figure 4 shows an image of an algae cell construct. The number of cells in each of the five clusters was counted, and the average number of cells per cluster, A, was calculated.

Step 2: The average number of algae cell clusters in the volume of a z-stack, B, was estimated. Three z-stacks were captured at three randomly chosen positions for each bioprinted construct. A z-stack is a combination of multiple cross-sectional images. Because each image is taken at a fixed depth interval within the sample, the z-stack is three-dimensional. The number of clusters in each of the three captured z-stacks were counted, and the average number of clusters per z-stack, B, was calculated.

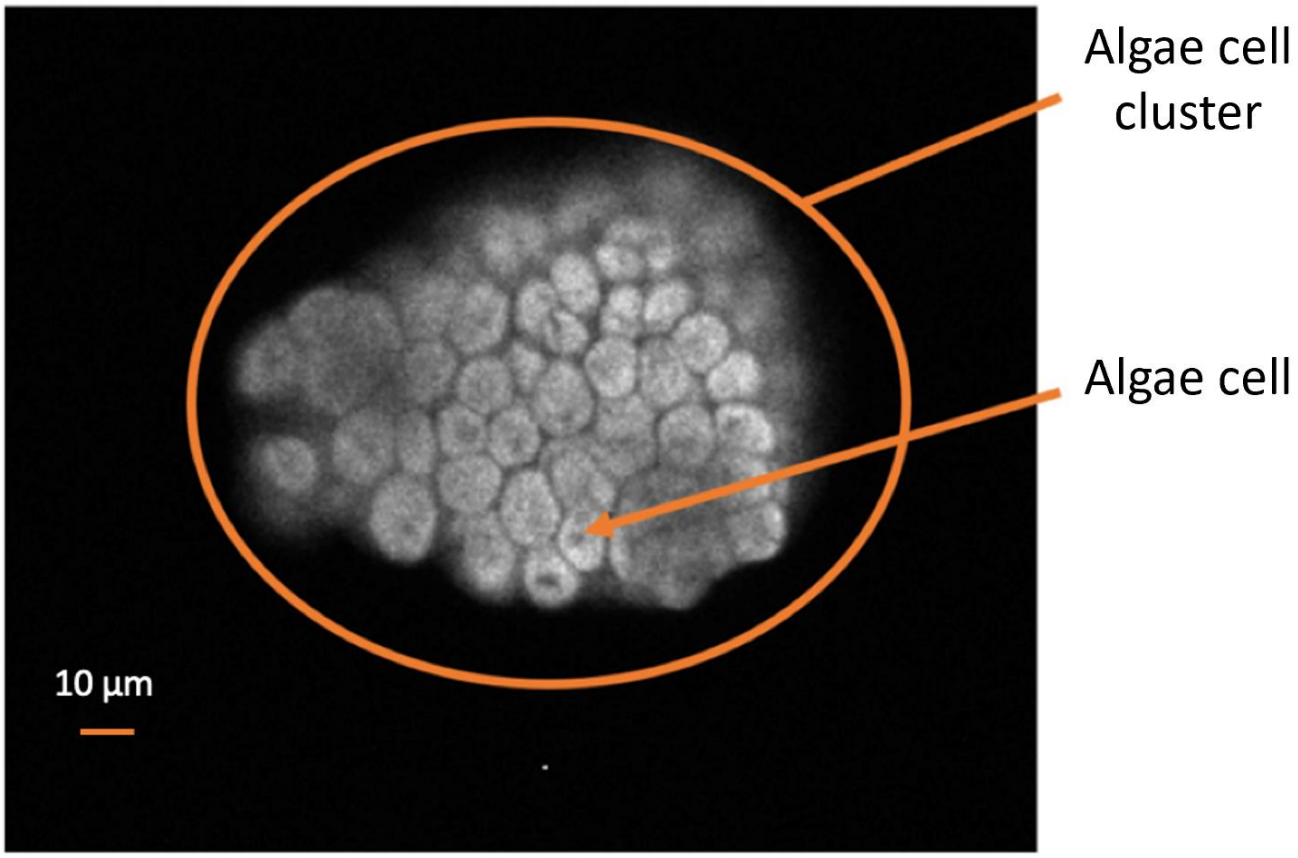

Figure 4. Confocal image of an algae cell cluster.

Step 3: The average z-stack volume, z, was estimated by multiplying the depth of each z-stack by the area covered by each image.

Step 4: The average concentration of cells per cubic millimeter (n) for each bioprinted construct was calculated using the following equation:

$$n = \frac{A.B.}{z}$$

Step 5: The average concentration of cells per cubic millimeter of bioprinted construct for each experimental condition, N, was calculated using the following equation:

$$N = \frac{n_1 + n_2 + n_3}{3}$$

2.2. Alginate:methylcellulose:GelMA Bioink Synthesis and Testing of Shear-thinning Behavior, Shape Fidelity, and Cell Viability

2.2.1. Algae Preparation

Algae was prepared following the same procedure as described in Section 2.1.1. After measuring the algae cell concentration in the TAP-algae solution using the Auto T4 cell counter, a centrifuge (Eppendorf, USA) was used to concentration the TAP-algae solution to a concentration of 10^7 cells/milliliter.

2.2.2. Alginate:methylcellulose:GelMA Synthesis

Bioink synthesis was performed in the dark to prevent crosslinking of the photoinitiator used in GelMA synthesis. In order to synthesize alginate:methylcellulose:GelMA, separate solutions of alginate:methylcellulose and GelMA were prepared, and the solutions were then combined. Alginate:methylcellulose was synthesized following the same procedure as described in Section

2.1.2. However, for this experiment, five grams of alginic acid sodium salt were added to the solution, one gram of methylcellulose was added to the solution, and 50 total milliliters of alginate:methylcellulose were synthesized. Additionally, algae cells were not added to the alginate:methylcellulose solution.

In order to synthesize GelMA, a 50-milliliter beaker was filled with 10 milliliters of deionized water and wrapped tightly with aluminum foil to block light and prevent evaporation. A magnetic stir bar was placed in the beaker, and the beaker was placed on a hot plate stirrer. The hot plate stirrer was heated to 60°C and the stirring speed was set to 500 rpm. While stirring, 0.1 grams of Igracure (Sigma-Aldrich, USA) was added to the beaker, and stirring continued for 30 minutes to allow the Igracure to completely dissolve. Afterwards, one gram of lyophilized GelMA (Allevi, USA) was added to the beaker and stirred for 1 hour at 500 rpm and 60°C.

After independently synthesizing the alginate:methylcellulose and GelMA solutions, 10 milliliters of alginate:methylcellulose were added to the beaker containing 10 milliliters of GelMA. The solution was stirred at 500 rpm at 60°C for 10 minutes to homogenously mix the alginate:methylcellulose and GelMA solutions. As a result, alginate:methylcellulose:GelMA bioink at a ratio of 5:1:5 (% w/v) was synthesized. The heat was then turned off for the hot plate stirrer to allow the solution to cool to 20°C. Algae-TAP solution was added to the alginate:methylcellulose:Gelma solution to synthesize bioink with an algae cell concentration of 10^6 cells/milliliter.

2.2.3. Rheological Analysis and Evaluation of Shear-thinning Behavior

Rheological analysis was performed to evaluate shear-thinning behavior of alginate:methylcellulose:GelMA bioink. The analysis was performed on an unprinted sample of bioink. TA Instrument DHR-2 rheometer (TA Instruments, USA) performed rotational shear-

viscosity measurements in flow mode on the alginate:methylcellulose:GelMA sample. The shear rate ranged from 0.01 to 700 1/s using the cone-plate system. The parameters for the experiment were set via the TRIOS software (TA Instruments, USA). All measurements were performed at 24 °C. Three repetitive measurements were obtained, as well as the average of the three measurements.

2.2.4. Construct Design

The 3D model of the construct was designed using a commercial CAD software (Solid-Works, Waltham, MA). The 3D model was in STL file format. The STL file was converted into G-code using Allevi Bioprint software (Allevi Inc, USA) prior to printing. The model was sliced with a layer thickness of 0.2 millimeters, had an edge length of 20 millimeters, had a grid infill pattern, and infill distance of 0.5 millimeters.

2.2.5. Bioprinting

Allevi 1 bioprinter (Allevi, USA) was used for bioprinting. Printing speed was set to 6 millimeters/second, extrusion pressure was set to 50 psi, and extrusion temperature was set to 21°C using the Allevi Bioprint software. Three replicates of the construct described in Section 2.2.4. were bioprinted. A needle with diameter of 210 μm was used to bioprint the constructs, and each construct was individually printed inside of a petri dish. Photo-crosslinking of the constructs was performed by UV lightbulbs contained in the bioprinter head, and the lightbulbs were controlled by the Allevi Bioprint software. After printing each layer of the constructs, UV light was used to photo-crosslink the constructs layer-by-layer. During photo-crosslinking, the UV light intensity was 7 mW/cm^2, and the constructs were exposed to UV light for 15 seconds after each layer was printed. After a construct was completely printed, it was exposed to UV light for an additional 45

seconds to ensure complete photo-crosslinking. After being photo-crosslinked, the alginate:methylcellulose:GelMA constructs were ionically crosslinked with 100 millimolar $CaCl_2$ for four minutes. The $CaCl_2$ was then removed from the petri dishes using Kimwipes.

2.2.6. Shape Fidelity Assessment

After bioprinting and crosslinking the three alginate:methylcellulose:GelMA constructs, the constructs were imaged using Dino-Lite AM73115MZT handheld microscope (Dino-Lite, USA) in conjunction with DinoCapture software. ImageJ software (ImageJ, USA) was used to take measurements of the construct images that were captured by the microscope. To assess the shape fidelity of the printed constructs, edge length, the length of the four edges of the construct on the top surface, was measured for each construct image, and this value was compared to the edge length of the CAD model used for bioprinting (20 millimeters). To calculate the average percentage deviation for edge length of the printed constructs, compared to the 20-millimeter edge length of the designed CAD model, the following equation was used:

$$Average\ percentage\ deviation = \frac{\sum_{i=1}^{4}\left(\frac{|l_i - 20|}{20}\right)}{4} * 100$$

2.2.7. Cell Viability Assessment

In this study, cell growth was used to measure cell viability. Cell growth was measured by comparing the concentration of algae cells in the bioprinted constructs four days post bioprinting to the initial concentration of algae cells in the bioink, 10^6 cells/milliliter. After shape fidelity measurements were taken of the three bioprinted constructs, as described in Section 2.2.6., liquid TAP medium was added to the petri dishes containing the constructs and the petri dishes were placed under lightbulbs for four days to promote algae cell growth.

The following procedure was used to evaluate algae cell growth in bioprinted constructs four days post bioprinting:

Step 1: The petri dishes that the constructs were bioprinted in were weighed before and after bioprinting to determine the weight of the bioprinted construct.

Step 2: After incubating under lightbulbs for four days, the constructs were transferred from the petri dishes to separate BD tubes (Becton Dickinson, USA). Each BD tube contained five milliliters of 0.9% NaCl (Sigma Aldrich, USA) and 55 mM sodium citrate (Sigma Aldrich, USA) solution [31]. The BD tubes were mixed by a vortex mixer (Sigma Aldrich, USA) at 1,000 rpm for ten minutes to dissolve the constructs.

Step 3: Auto T4 cell counter was used to measure the concentration of the algae cells in the dissolved constructs, according to the instructions from the cell counter manufacturer. A solution of 0.2% trypan blue (Fisher Scientific, USA) was added to the BD tubes containing the dissolved constructs at a 1:1 ratio before using the Auto T4 cell counter. Dead cells were stained blue, allowing them to be differentiated from live cells by the cell counter. The volume of each construct was determined using the weight of the construct, determined in step 1, and the density of the alginate:methylcellulose:GelMA bioink. The cell concentration of each bioprinted construct before being dissolved was determined using the data from Auto T4 cell counter, the volume of the construct before being dissolved, and the volume of the construct after being dissolved.

3. RESULTS

3.1. Determining the Effects of Variable Extrusion Pressure and Nozzle Diameter on the Cell Viability of Green Bioprinted Constructs

3.1.1 Effects of Extrusion Pressure

The algae cell concentration data for the extrusion pressure experiment is shown in Table 1. A two-factor analysis of variance (ANOVA) was conducted on the cell concentration data to determine if there are significant differences in algae cell concentration based on the value of extrusion pressure used during bioprinting and the number of days post bioprinting. The ANOVA also tested for interaction effects between the extrusion pressure value and number of days post bioprinting on algae cell concentration of bioprinted constructs. The significance level of 0.05 was chosen for the ANOVA. The results of the ANOVA are shown in Table 2. The results of the ANOVA indicate that the main effects of extrusion pressure value, the main effects of the number of days post bioprinting, and the interaction effects of these factors all significantly affect the cell concentration of bioprinted constructs. Figure 5 graphically depicts the cell concentrations of the bioprinted constructs in the extrusion pressure experiment.

The data analysis reveals that cell concentration decreases as extrusion pressure increases. Cell concentration increased between day 3 and day 6 for all bioprinted constructs. However, the constructs bioprinted with higher extrusion pressures had smaller rates of cell growth. From the data, it can be concluded that the cell viability of green bioprinted constructs decreases as extrusion pressure increases.

Table 1. Cell concentration (1000/mm^3) in constructs printed at different levels of extrusion pressure.

Number of Days Post Bioprinting	Extrusion Pressure (Bar)	Replicant 1	Replicant 2	Replicant 3	Mean	Standard Deviation
3	3	8.341	7.912	7.880	8.044	0.601
3	5	5.912	5.414	6.876	6.068	0.922
3	7	3.984	3.840	3.895	3.907	0.658
6	3	28.130	23.383	23.808	25.107	2.984
6	7	13.217	14.171	15.638	14.342	1.323
6	5	9.989	9.801	8.384	9.391	0.921

Table 2. Results of the two-factor ANOVA conducted for extrusion pressure and the number of days post bioprinting.

Source	DF	Adj SS	Adj MS	F-value	P-value
Pressure	2	3418227	1709113	223.81	0.000
Number of Days	1	2812007	2812007	368.23	0.000
Pressure*Day	2	1005553	502777	65.84	0.000
Error	54	412372	7637		
Total	59	7648159			

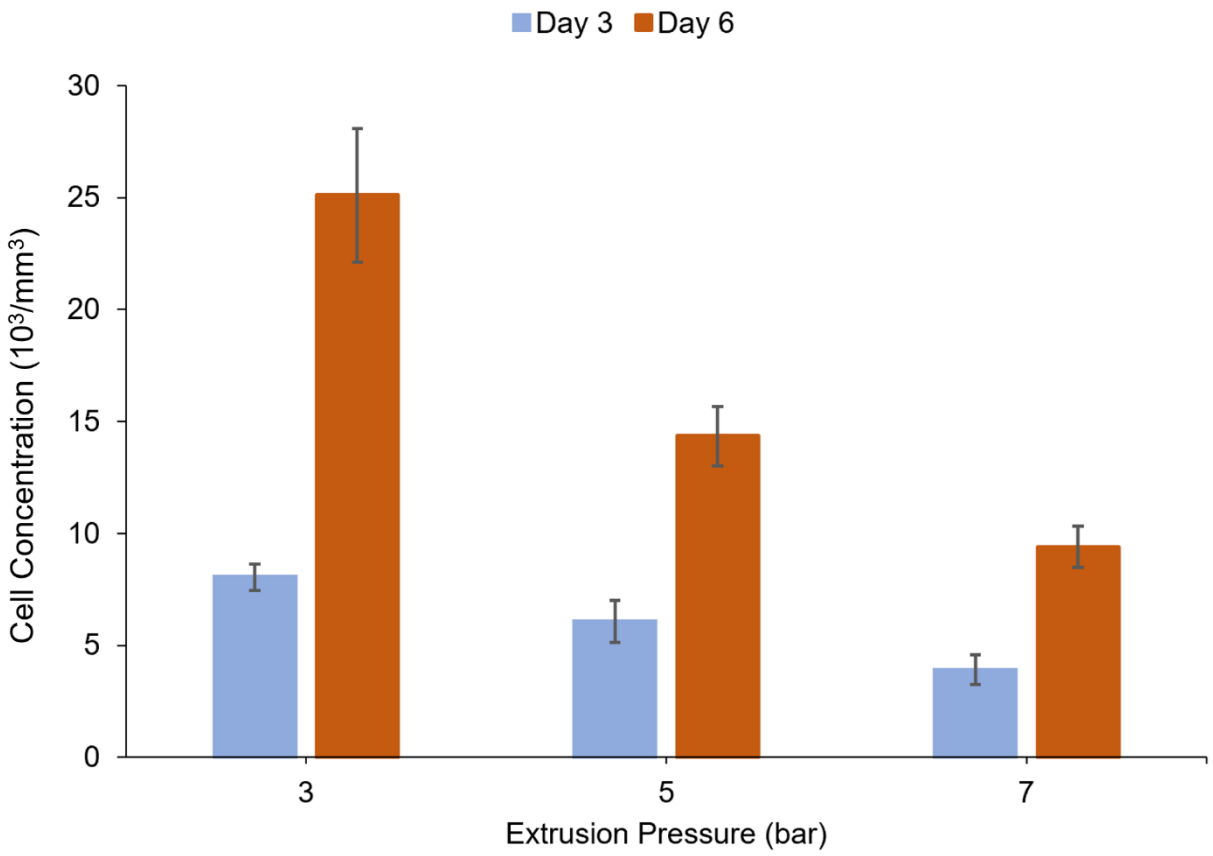

Figure 5. Effect of extrusion pressure and number of days post bioprinting on algae cell concentration.

3.1.2 Effects of Nozzle Diameter

The algae cell concentration data for the nozzle diameter experiment is shown in Table 3. An ANOVA was conducted the same way as described in Section 3.1.1., and 0.05 was chosen as the significance level. The results of the ANOVA are shown in Table 4. The ANOVA indicates that the main effects of nozzle diameter value, the main effects of the number of days post bioprinting, and the interaction effects of these factors all significantly affect the cell concentration of green bioprinted constructs. Figure 5 graphically depicts the cell concentrations of the bioprinted constructs in the nozzle diameter experiment.

As shown by the data, cell concentration decreases as nozzle diameter decreases. Although cell concentration increased between day 3 and day 6 for all bioprinted constructs. However, the rate of cell growth was negatively affected for constructs bioprinted with smaller nozzle diameters. From the data, it can be concluded that the cell viability of green bioprinted constructs decreases as nozzle diameter decreases.

Table 3. Cell concentration (1000/mm^3) in constructs printed at different levels of nozzle diameter.

Number of Days Post Biorinting	Nozzle Diameter (μm)	Replicant 1	Replicant 2	Replicant 3	Mean	Standard Deviation
3	200	5.188	4.923	4.573	4.895	0.308
3	250	6.024	6.868	6.273	6.388	0.433
3	400	9.353	8.768	8.828	8.983	0.321
6	200	9.989	9.982	9.473	9.815	0.295
6	250	13.194	13.942	13.645	13.594	0.376
6	400	26.586	22.633	22.247	23.822	2.400

Table 4. Results of the two-factor ANOVA conducted for nozzle diameter and the number of days post bioprinting.

Source	DF	Adj SS	Adj MS	F-value	P-value
Nozzle	2	3.296×10^{14}	1.648×10^{14}	80.92	0.000
Number of Days	1	2.812×10^{14}	2.812×10^{14}	312.09	0.000
Nozzle*Day	2	9.49×10^{13}	4.745×10^{13}	89.86	0.000
Error	54	1375894	24570		
Total	59	7340138			

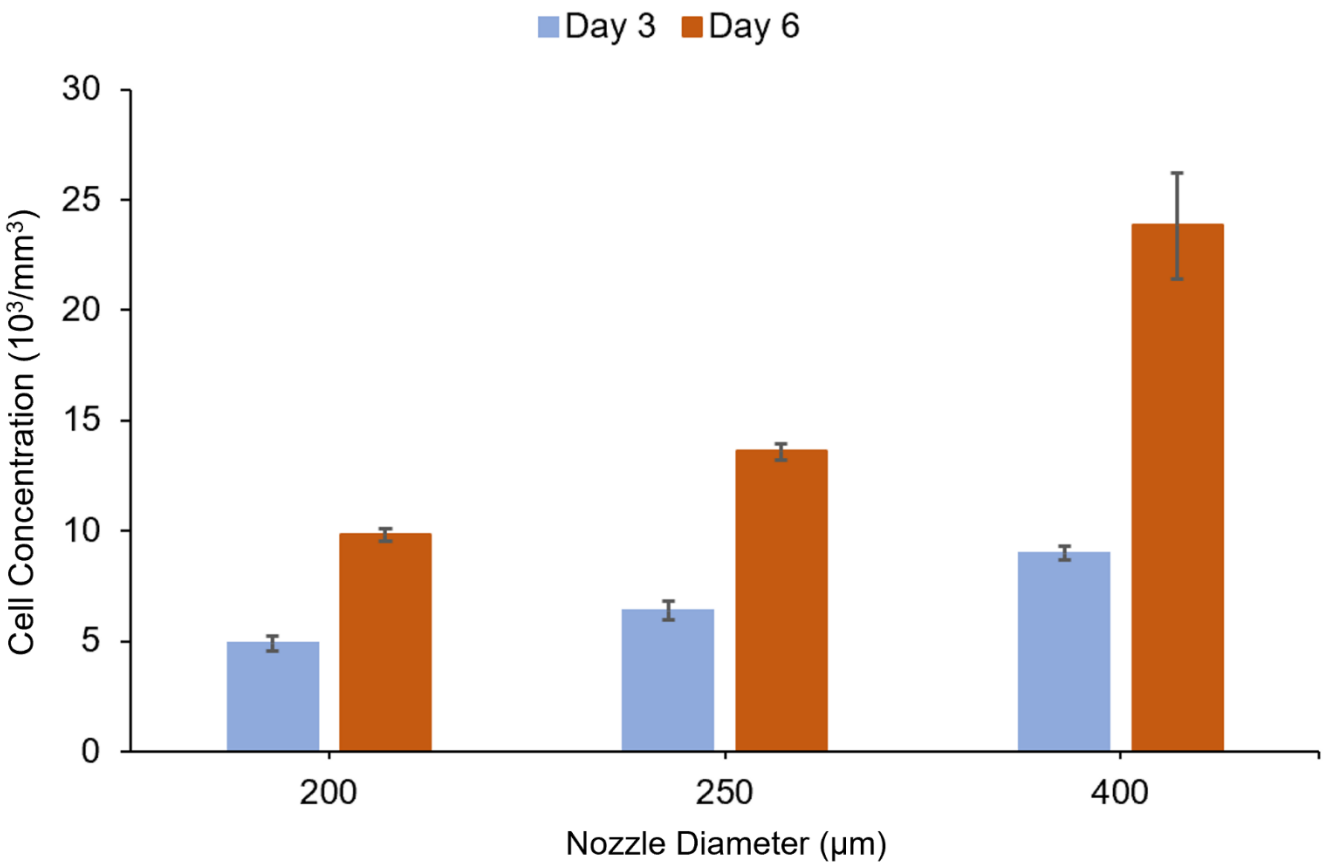

Figure 6. Effect of nozzle diameter and number of days post bioprinting on algae cell concentration.

3.2. Alginate:methylcellulose:GelMA Bioink Synthesis and Testing of Shear-thinning Behavior, Shape Fidelity, and Cell Viability

The results of the rheological analysis, which determines if a bioink exhibits shear-thinning behavior, are shown in Figure 7. As shear rate increased, the viscosity of the bioink decreased. The viscosity of the bioink significantly decreased when shear rate was around 20 1/s. Because alginate:methylcellulose:GelMA has high viscosity at low shear rates and low viscosity at high shear rates, the bioink exhibits shear-thinning behavior.

The measured edge length data of the three alginate:methylcellulose:GelMA constructs is shown in Table 5. Figure 8 shows the average percent deviation of edge length for each bioprinted construct compared to the CAD model. The data reveals variation in edge length between the three bioprinted constructs. The highest observed percent deviation was 10.696%, and the lowest observed percent deviation was 2.295%. From the data, it can be expected that the shape fidelity of alginate:methylcellulose:GelMA bioprinted constructs could deviate from the CAD model by between approximately 2% to 11%.

The cell concentration data is shown in Table 6. Figure 9 compares the cell concentration of the three bioprinted constructs four days post bioprinting to the initial cell concentration of the bioink, 10^6 cells/milliliter. The cell concentration increased in all bioprinted constructs, indicating cell growth occurred and the cells in the constructs are viable. For all bioprinted constructs, the cell concentration at least doubled four days post bioprinting.

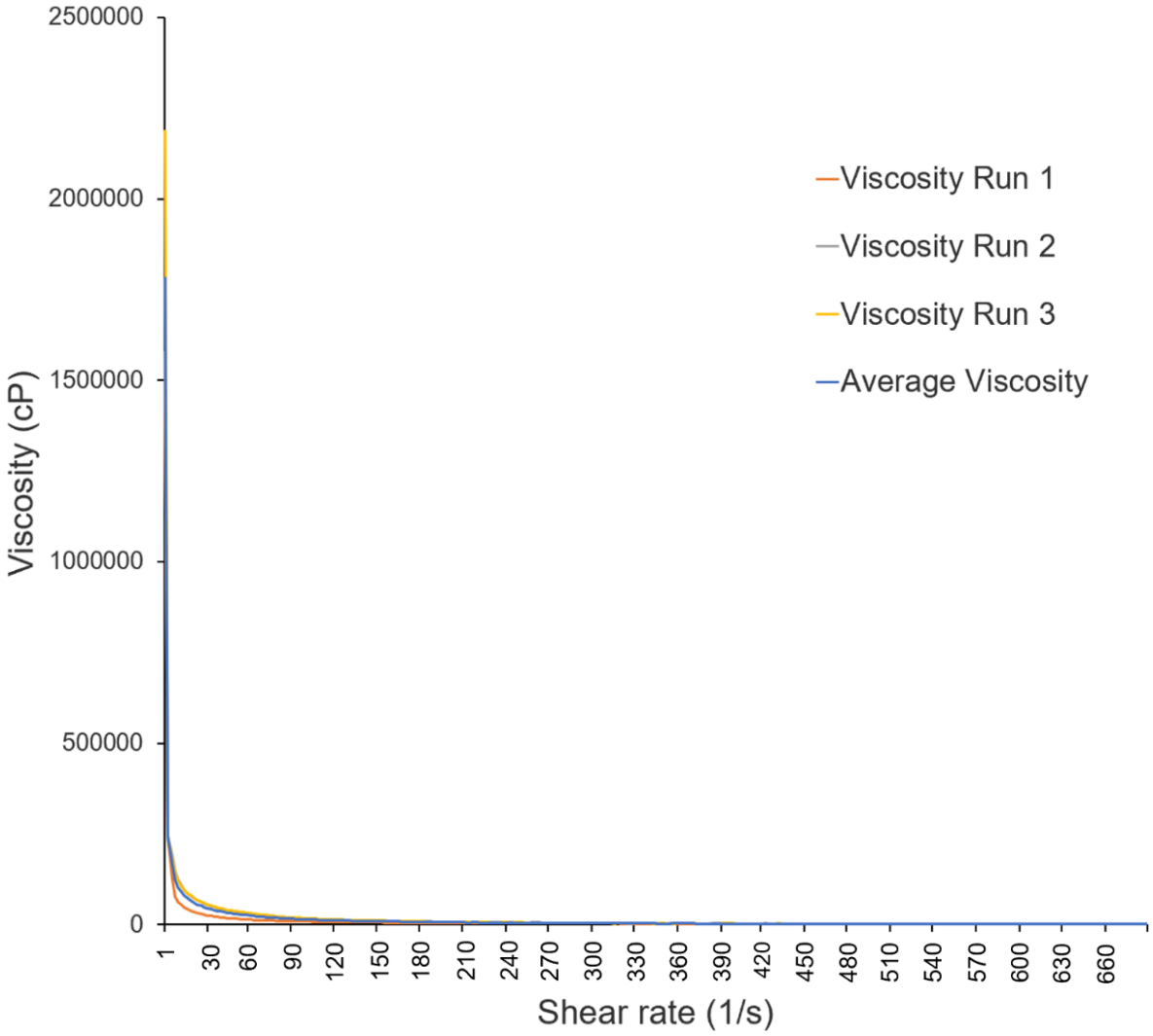

Figure 7. Relationship between viscosity and shear rate for alginate:methylcellulose:GelMA.

Table 5. Edge length measurements of alginate:methylcellulose:GelMA bioprinted constructs and average percent deviation from CAD model.

Replicate number	Edge length 1 (millimeters)	Edge length 2 (millimeters)	Edge length 3 (millimeters)	Edge length 4 (millimeters)	Average percent deviation from CAD model (%)
Replicate 1	21.461	22.852	21.657	22.587	10.696
Replicate 2	21.669	22.202	22.001	21.592	9.33
Replicate 3	20.780	20.046	20.902	20.108	2.295

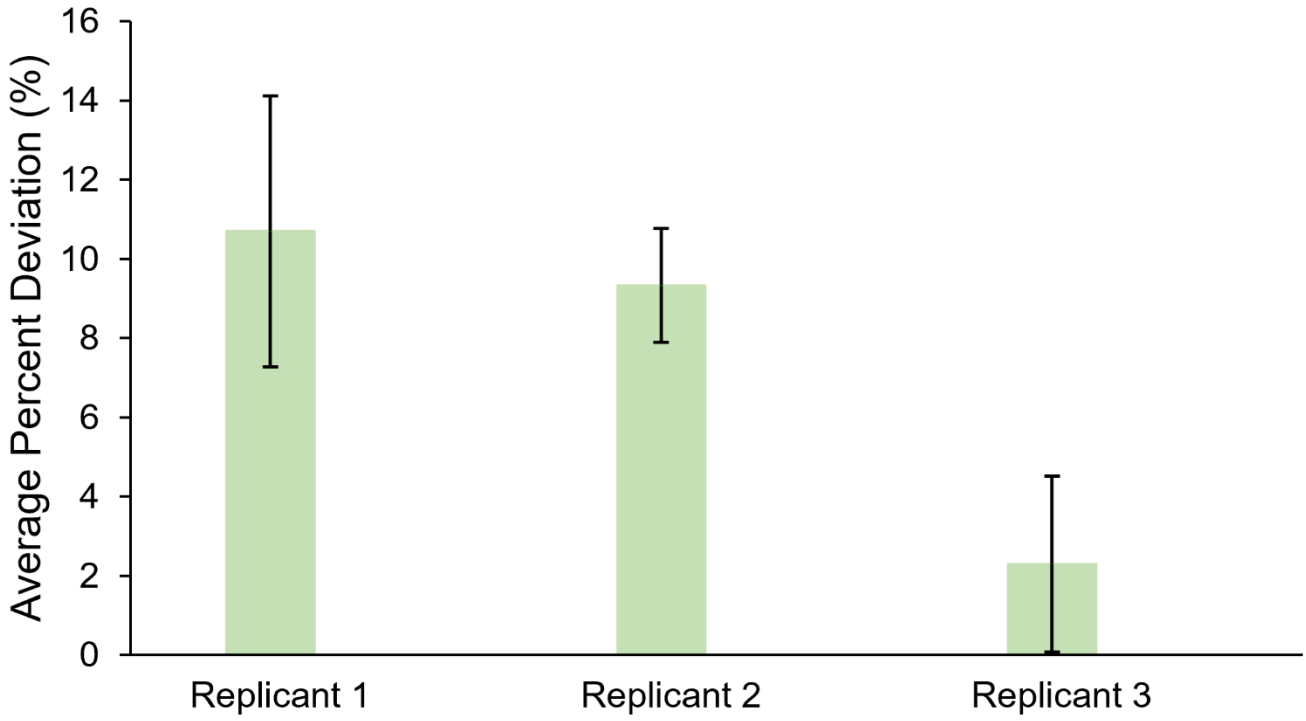

Figure 8. The average edge length percent deviations of the three alginate:methylcellulose:GelMA constructs.

Table 6. Cell concentration measurements four days post bioprinting of the three alginate:methylcellulose:GelMA constructs.

Replicate number	Cell concentration (cells/milliliter)
Replicant 1	2,110,000
Replicant 2	2,820,000
Replicant 3	2,650,000

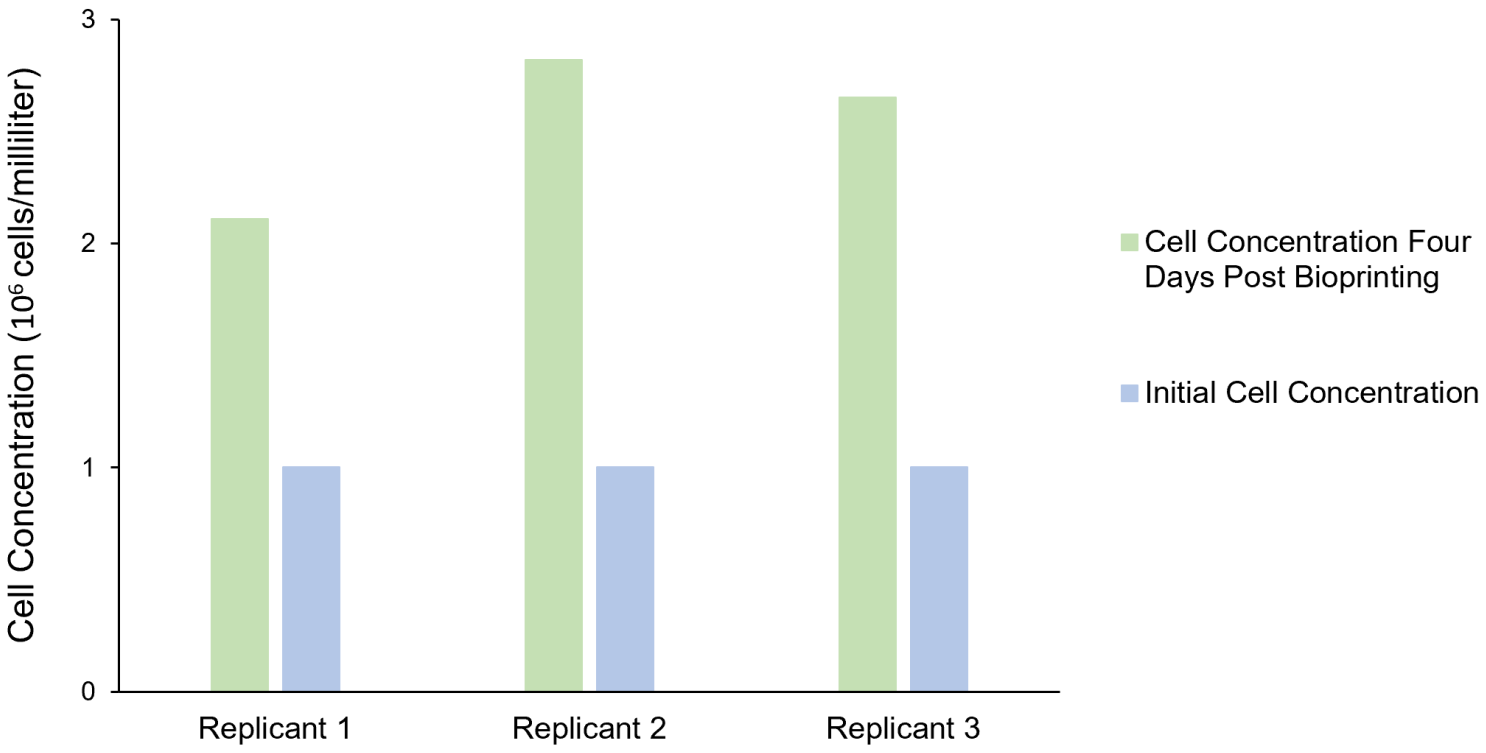

Figure 9: Comparison of cell concentration in alginate:methylcellulose:GelMA constructs four days post bioprinting to initial cell concentration.

4. DISCUSSION

4.1. Determining the Effects of Variable Extrusion Pressure and Nozzle Diameter on the Cell Viability of Green Bioprinted Constructs

The collected data indicates that *Chlamydomonas reinhardtii* algae cell concentration in green bioprinted constructs decreases as extrusion pressure values increase. Conversely, algae cell concentration decreases as nozzle diameter values decrease. The results from both these experiments are consistent with previous studies that have measured the effects of extrusion pressure [52 – 54] and nozzle diameter [53 – 55] on mammalian cell viability in bioprinted constructs. In extrusion-based bioprinting, shear stress is applied to cells within the bioink as bioink is extruded [15]. Furthermore, increasing extrusion pressure and decreasing nozzle diameter increase the amount of shear stress applied during bioprinting [26], which can damage bioprinted cells [26]. Although the presence of a cell wall increases the structural integrity of photosynthetic cells compared to mammalian cells [57], the data from the extrusion pressure and nozzle diameter experiments indicate that the harmful effects of shear stress on cell viability affect photosynthetic cells in green bioprinted constructs.

The algae cell concentration in the bioprinted constructs were measured both three days and six days post bioprinting to determine the effects of variable extrusion pressure and nozzle diameter values over time. In addition to lower cell concentrations, the rate of algae cell growth was smaller between day 3 and day 6 post bioprinting under conditions with high shear stress, either from high extrusion pressure or small nozzle diameter. Because cell growth occurred between day 3 and day 6 for all bioprinted constructs, some quantity of living algae cells was present in all of the constructs post bioprinting. However, the smaller rate of cell growth for the

high shear stress conditions suggests that cellular damage caused by shear stress can impact the cell viability of bioprinted constructs for at least six days post bioprinting.

Trade-offs must be made when selecting parameter values for use in bioprinting. Sufficiently high extrusion pressure is required during extrusion-based bioprinting to ensure the printing nozzle does not become clogged [58], despite high extrusion pressure values decreasing cell viability. Additionally, although large nozzle diameters do not decrease cell viability, these diameters are unable to bioprint constructs with high shape fidelity [15]. For these reasons, bioprinting researchers must consider the balance between printability, shape fidelity, and cell viability when selecting parameter values.

4.2. Alginate:methylcellulose:GelMA Bioink Synthesis and Testing of Shear-thinning Behavior, Shape Fidelity, and Cell Viability

In order for a bioink to be compatible with extrusion-based bioprinting, it must exhibit shear-thinning behavior [16]. Because extrusion-based bioprinting is one of the main bioprinting techniques currently in use [11], shear-thinning behavior is a critical property a newly developed bioink must possess. Rheological analysis results of the new bioink alginate:methylcellulose:GelMA indicate the viscosity of the bioink decreases as shear stress increases, and the viscosity of the bioink increases and shear stress decreases. These results confirm that alginate:methylcellulose:GelMA exhibits shear-thinning behavior, and is compatible with the extrusion-based bioprinting technique.

In order to determine if alginate:methylcellulose:GelMA bioink is capable of bioprinting constructs with high shape fidelity, the edge lengths of three alginate:methylcellulose:GelMA bioprinted constructs were measured, and the lengths were compared to the CAD model edge

length. The percent deviation of the bioprinted construct edge lengths ranged from approximately 2% to 11%. A percent deviation of 0% would indicate that the bioprinted constructs perfectly match the shape of the CAD model. To determine if the alginate:methylcellulose:GelMA constructs have acceptable shape fidelity, the percent deviations of the bioprinted constructs were compared to the percent deviations of constructs bioprinted with other photo-crosslinkable bioinks in the literature. Table 7 shows a shape fidelity comparison between alginate:methylcellulose:GelMA bioink and other photo-crosslinkable bioinks. Even among photo-crosslinkable bioinks, which tend to bioprint constructs of high shape fidelity [47], there is considerable variation in the accuracy of bioprinted constructs to the CAD model. Because the percent deviation of the alginate:methylcellulose:GelMA bioprinted constructs is within the range acceptable for other photo-crosslinkable bioinks, alginate:methylcellulose:GelMA is concluded to bioprint constructs of acceptable shape fidelity.

In order to determine the cell viability of constructs bioprinted with alginate:methylcellulose:GelMA, the cell concentration in bioprinted constructs was measured four days post bioprinting and compared to the initial concentration of cells in the bioink. The initial cell concentration was 10^6 cells/milliliter, and the cell concentration more than doubled after four days in each of the three alginate:methylcellulose:GelMA bioprinted constructs. The algae cell growth in the alginate:methylcellulose:GelMA constructs was not as drastic as the cell growth in constructs bioprinted with alginate:methylcellulose [30, 31] and alginate:agarose:methylcellulose [37]. However, alginate:methylcellulose:GelMA is a photo-crosslinkable bioink and contains GelMA, a synthetically derived component. Both of these factors are associated with lower cell viability in bioprinted constructs [16, 47].

Table 7: Comparison of alginate:methylcellulose:GelMA shape fidelity measurements to the shape fidelity measurements of other photo-crosslinkable bioinks.

Bioink	CAD model dimension (millimeters)	Printed construct dimension (millimeters)	Average percent deviation (%)	Reference
Alginate:methylcellulose:GelMA	20	20.046 – 22.852	2.295 – 10.696	-
GelMA	0.30	0.50 – 0.55	66.67 – 83.33	[59]
GelMA-gellan gum	0.25	0.344 – 0.745	37.60 – 198	[60]
Poly-(propylene fumarate)	0.25	0.1 – 1.1	0 – 340	[61]

Despite these potential cell viability disadvantages, the algae cells in alginate:methylcellulose:GelMA bioink survived the bioprinting and crosslinking processes, and were capable of growth and reproduction. For these reasons, constructs bioprinted with alginate:methylcellulose:GelMA bioink are concluded to have sufficient cell viability.

The collected data during experimentation with the novel alginate:methylcellulose:GelMA bioink confirms that the bioink is suitable for use in green bioprinting. Alginate:methylcellulose:GelMA is the first photo-crosslinkable bioink proven to be compatible with green bioprinting, and is the third bioink overall proven to be compatible with green bioprinting. Because of the high structural integrity and shape fidelity of photo-crosslinkable bioinks [16], including alginate:methylcellulose:GelMA, the introduction of this bioink will allow green constructs with more complex geometries to be bioprinted.

4.3 Broader Impacts of Conducted Research

The data gathered during the extrusion pressure and nozzle diameter experiments is the first to study the effects of printing parameters on cell viability in green bioprinted constructs. Additionally, the results of these experiments helped inform the materials and methods of a separate study published by the research group [38]. The separate study examined the feasibility of removing copper from water using alginate:methylcellulose bioprinted filters containing *Chlamydomonas reinhardtii* algae cells. The results from the study were promising, and act as a proof-of-concept for the usage of green bioprinted constructs in environmental remediation. The effects of extrusion pressure and nozzle diameter on the cell viability of green bioprinted constructs may serve as a guideline for selecting printing parameter values in additional future green bioprinting experiments.

A publication is currently being drafted which details the data gathered during alginate:methylcellulose:GelMA experimentation, including the results of shear-thinning behavior, shape fidelity, and cell viability. Three additional experiments have since been conducted by the research group using the new alginate:methylcellulose:GelMA bioink. The feasible regions of alginate:methylcellulose:GelMA have been determined, similarly to a previous experiment performed by the research group to determine the feasible regions of alginate:methylcellulose [58]. Feasible regions describe the combination of printing parameters that are necessary in order for a continuous strand of a bioink to be bioprinted [58]. A separate experiment was conducted to determine the effects of extrusion pressure, nozzle diameter, and bioink composition on the shape fidelity and cell viability of constructs bioprinted with alginate:methylcellulose:GelMA bioink. Because alginate:methylcellulose:GelMA is a photo-crosslinkable bioink, an additional experiment was conducted to determine the effects of UV light exposure time and intensity on shape fidelity and cell viability of constructs bioprinted with alginate:methylcellulose:GelMA bioink. Publications are currently being drafted for each of these three experiments.

In addition to the planned publications utilizing alginate:methylcellulose:GelMA bioink, a patent application has been submitted to the Texas A&M patent office. The bioink was deemed to have sufficient novelty by the patent office to continue with the patent filing process. The research group is currently awaiting the filing of a provisional patent.

5. CONCLUSIONS

For the first time, the effects of printing parameters on photosynthetic cell viability in green bioprinted constructs were studied by varying the values of extrusion pressure and nozzle diameter used during extrusion-based bioprinting. It can be concluded that the viability of photosynthetic cells in green bioprinted constructs is negatively affected by bioprinting conditions with higher shear stress, including increasing extrusion pressure and decreasing nozzle diameter. These trends have previously been observed in bioprinting involving mammalian cells. Because high extrusion pressures and small nozzle diameters are beneficial for other aspects of green bioprinting, researchers must carefully choose bioprinting parameter values that balance printability, shape fidelity, and cell viability of bioprinted constructs. Future research is required in order to understand the effects of additional parameter values on the cell viability of green bioprinted constructs, including extrusion temperature, bioprinting speed, and bioink composition.

A new bioink, alginate:methylcellulose:GelMA, was synthesized for use in green bioprinting, and is the first photo-crosslinkable bioink proven to be compatible with green bioprinting. Alginate:methylcellulose:GelMA bioprinted constructs had high shape fidelity, and were comparable to the shape fidelities of constructs bioprinted with other photo-crosslinkable bioinks. The algae cells within the alginate:methylcellulose:GelMA constructs survived the processes of bioprinting and crosslinking, and were capable of growth and reproduction. The new bioink is also compatible with the extrusion-based bioprinting technique because the bioink exhibits shear-thinning behavior.

REFERENCES

[1] Thayer, P., Martinez, H. and Gatenholm, E., 2020. History and trends of 3D bioprinting. In *3D Bioprinting* (pp. 3-18). Humana, New York, NY.

[2] Sun, T., Jackson, S., Haycock, J.W. and MacNeil, S., 2006. Culture of skin cells in 3D rather than 2D improves their ability to survive exposure to cytotoxic agents. *Journal of biotechnology*, *122*(3), pp.372-381.

[3] Yamada, K.M. and Cukierman, E., 2007. Modeling tissue morphogenesis and cancer in 3D. *Cell*, *130*(4), pp.601-610.

[4] Griffith, L.G. and Swartz, M.A., 2006. Capturing complex 3D tissue physiology in vitro. *Nature reviews Molecular cell biology*, *7*(3), pp.211-224.

[5] Breslin, S. and O'Driscoll, L., 2016. The relevance of using 3D cell cultures, in addition to 2D monolayer cultures, when evaluating breast cancer drug sensitivity and resistance. *Oncotarget*, *7*(29), p.45745.

[6] Begley, C.G. and Ellis, L.M., 2012. Raise standards for preclinical cancer research. *Nature*, *483*(7391), pp.531-533.

[7] Huang, Y., Zhang, X.F., Gao, G., Yonezawa, T. and Cui, X., 2017. 3D bioprinting and the current applications in tissue engineering. *Biotechnology journal*, *12*(8), p.1600734.

[8] Nie, J., Gao, Q., Fu, J. and He, Y., 2020. Grafting of 3D bioprinting to in vitro drug screening: a review. *Advanced healthcare materials*, *9*(7), p.1901773.

[9] Mandrycky, C., Wang, Z., Kim, K. and Kim, D.H., 2016. 3D bioprinting for engineering complex tissues. *Biotechnology advances*, *34*(4), pp.422-434.

[10] Memic, A., Navaei, A., Mirani, B., Cordova, J.A.V., Aldhahri, M., Dolatshahi-Pirouz, A., Akbari, M. and Nikkhah, M., 2017. Bioprinting technologies for disease modeling. *Biotechnology letters*, *39*(9), pp.1279-1290.

[11] Cho, D.W., Kim, B.S., Jang, J., Gao, G., Han, W. and Singh, N.K., 2019. 3D bioprinting techniques. In *3D Bioprinting* (pp. 25-29). Springer, Cham.

[12] Pakhomova, C., Popov, D., Maltsev, E., Akhatov, I. and Pasko, A., 2020. Software for bioprinting. *International Journal of Bioprinting*, *6*(3).

[13] Gao, G., Kim, B.S., Jang, J. and Cho, D.W., 2019. Recent strategies in extrusion-based three-dimensional cell printing toward organ biofabrication. *ACS Biomaterials Science & Engineering*, *5*(3), pp.1150-1169.

[14] Gou, M., Qu, X., Zhu, W., Xiang, M., Yang, J., Zhang, K., Wei, Y. and Chen, S., 2014. Bio-inspired detoxification using 3D-printed hydrogel nanocomposites. *Nature communications*, *5*(1), pp.1-9.

[15] Ozbolat, I.T. and Hospodiuk, M., 2016. Current advances and future perspectives in extrusion-based bioprinting. *Biomaterials*, *76*, pp.321-343.

[16] Hospodiuk, M., Dey, M., Sosnoski, D. and Ozbolat, I.T., 2017. The bioink: A comprehensive review on bioprintable materials. *Biotechnology advances*, *35*(2), pp.217-239.

[17] Wilson, S.A., Cross, L.M., Peak, C.W. and Gaharwar, A.K., 2017. Shear-thinning and thermo-reversible nanoengineered inks for 3D bioprinting. *ACS applied materials & interfaces*, *9*(50), pp.43449-43458.

[18] Li, H., Tan, Y.J., Leong, K.F. and Li, L., 2017. 3D bioprinting of highly thixotropic alginate/methylcellulose hydrogel with strong interface bonding. *ACS applied materials & interfaces*, *9*(23), pp.20086-20097.

[19] Duan, B., Hockaday, L.A., Kang, K.H. and Butcher, J.T., 2013. 3D bioprinting of heterogeneous aortic valve conduits with alginate/gelatin hydrogels. *Journal of biomedical materials research Part A*, *101*(5), pp.1255-1264.

[20] Dababneh, A.B. and Ozbolat, I.T., 2014. Bioprinting technology: a current state-of-the-art review. *Journal of Manufacturing Science and Engineering*, *136*(6).

[21] Murphy, S.V. and Atala, A., 2014. 3D bioprinting of tissues and organs. *Nature biotechnology*, *32*(8), pp.773-785.

[22] Guillotin, B., Souquet, A., Catros, S., Duocastella, M., Pippenger, B., Bellance, S., Bareille, R., Rémy, M., Bordenave, L., Amédée, J. and Guillemot, F., 2010. Laser assisted bioprinting of engineered tissue with high cell density and microscale organization. *Biomaterials*, *31*(28), pp.7250-7256.

[23] Mironov, V., Kasyanov, V. and Markwald, R.R., 2011. Organ printing: from bioprinter to organ biofabrication line. *Current opinion in biotechnology*, *22*(5), pp.667-673.

[24] Marga, F., Jakab, K., Khatiwala, C., Shepherd, B., Dorfman, S., Hubbard, B., Colbert, S. and Forgacs, G., 2012. Toward engineering functional organ modules by additive manufacturing. *Biofabrication*, *4*(2), p.022001.

[25] Xu, T., Gregory, C.A., Molnar, P., Cui, X., Jalota, S., Bhaduri, S.B. and Boland, T., 2006. Viability and electrophysiology of neural cell structures generated by the inkjet printing method. *Biomaterials*, *27*(19), pp.3580-3588.

[26] Chang, R., Nam, J. and Sun, W., 2008. Effects of dispensing pressure and nozzle diameter on cell survival from solid freeform fabrication–based direct cell writing. *Tissue Engineering Part A*, *14*(1), pp.41-48.

[27] Guillemot, F., Souquet, A., Catros, S., Guillotin, B., Lopez, J., Faucon, M., Pippenger, B., Bareille, R., Rémy, M., Bellance, S. and Chabassier, P., 2010. High-throughput laser printing of cells and biomaterials for tissue engineering. *Acta biomaterialia*, *6*(7), pp.2494-2500.

[28] Kim, J.D., Choi, J.S., Kim, B.S., Choi, Y.C. and Cho, Y.W., 2010. Piezoelectric inkjet printing of polymers: Stem cell patterning on polymer substrates. *Polymer*, *51*(10), pp.2147-2154.

[29] Chang, C.C., Boland, E.D., Williams, S.K. and Hoying, J.B., 2011. Direct-write bioprinting three-dimensional biohybrid systems for future regenerative therapies. *Journal of Biomedical Materials Research Part B: Applied Biomaterials*, *98*(1), pp.160-170.

[30] Lode, A., Krujatz, F., Brüggemeier, S., Quade, M., Schütz, K., Knaack, S., Weber, J., Bley, T. and Gelinsky, M., 2015. *Green bioprinting: Fabrication of photosynthetic algae-laden hydrogel scaffolds for biotechnological and medical applications* (Vol. 15, No. 2, pp. 177-183).

[31] Krujatz, F., Lode, A., Brüggemeier, S., Schütz, K., Kramer, J., Bley, T., Gelinsky, M. and Weber, J., 2015. Green bioprinting: Viability and growth analysis of microalgae immobilized in 3D-plotted hydrogels versus suspension cultures. *Engineering in Life Sciences*, *15*(7), pp.678-688.

[32] Campostrini, R., Carturan, G., Caniato, R., Piovan, A., Filippini, R., Innocenti, G. and Cappelletti, E.M., 1996. Immobilization of plant cells in hybrid sol-gel materials. *Journal of Sol-Gel Science and Technology*, *7*(1), pp.87-97.

[33] Kallscheuer, N., Classen, T., Drepper, T. and Marienhagen, J., 2019. Production of plant metabolites with applications in the food industry using engineered microorganisms. *Current opinion in biotechnology*, *56*, pp.7-17.

[34] Haas, P. and Hill, T.G., 1932. The occurrence of sugar alcohols in marine algae: Sorbitol. *Biochemical Journal*, *26*(4), p.987.

[35] Aksu, Z., Eğretli, G., and Kutsal, T., "A comparative study of copper (II) biosorption on Ca-alginate, agarose and immobilized C. vulgaris in a packed-bed column," Process Biochemistry, 33(4), pp. 393-400, 1998.

[36] Bajpai, S.K., and Sharma, S., “Investigation of swelling/degradation behaviour of alginate beads crosslinked with Ca2+ and Ba2+ ions,” Reactive and Functional Polymers, 59(2), pp.129-140, 2004.

[37] Seidel, J., Ahlfeld, T., Adolph, M., Kümmritz, S., Steingroewer, J., Krujatz, F., Bley, T., Gelinsky, M. and Lode, A., 2017. Green bioprinting: extrusion-based fabrication of plant cell-laden biopolymer hydrogel scaffolds. *Biofabrication*, *9*(4), p.045011.

[38] Thakare, K., Jerpseth, L., Pei, Z., Tomlin, B. and Qin, H., 2021. Three-Dimensional Printing of Hydrogel Filters Containing Algae Cells for Copper Removal From Contaminated Water. *Journal of Manufacturing Science and Engineering*, *143*(10), p.104502.

[39] Groll, J., Burdick, J.A., Cho, D.W., Derby, B., Gelinsky, M., Heilshorn, S.C., Juengst, T., Malda, J., Mironov, V.A., Nakayama, K. and Ovsianikov, A., 2018. A definition of bioinks and their distinction from biomaterial inks. *Biofabrication*, *11*(1), p.013001.

[40] Chimene, D., Kaunas, R. and Gaharwar, A.K., 2020. Hydrogel bioink reinforcement for additive manufacturing: a focused review of emerging strategies. *Advanced materials*, *32*(1), p.1902026.

[41] Yamamoto, M., James, D., Li, H., Butler, J., Rafii, S. and Rabbany, S., 2010. Generation of stable co-cultures of vascular cells in a honeycomb alginate scaffold. *Tissue Engineering Part A*, *16*(1), pp.299-308.

[42] Gasperini, L., Mano, J.F. and Reis, R.L., 2014. Natural polymers for the microencapsulation of cells. *Journal of the royal society Interface*, *11*(100), p.20140817.

[43] Lee, K.Y. and Mooney, D.J., 2012. Alginate: properties and biomedical applications. *Progress in polymer science*, *37*(1), pp.106-126.

[44] Zhu, J. and Marchant, R.E., 2011. Design properties of hydrogel tissue-engineering scaffolds. *Expert review of medical devices*, *8*(5), pp.607-626.

[45] Raphael, B., Khalil, T., Workman, V.L., Smith, A., Brown, C.P., Streuli, C., Saiani, A. and Domingos, M., 2017. 3D cell bioprinting of self-assembling peptide-based hydrogels. *Materials Letters*, *190*, pp.103-106.

[46] Slaughter, B.V., Khurshid, S.S., Fisher, O.Z., Khademhosseini, A. and Peppas, N.A., 2009. Hydrogels in regenerative medicine. *Advanced materials*, *21*(32-33), pp.3307-3329.

[47] GhavamiNejad, A., Ashammakhi, N., Wu, X.Y. and Khademhosseini, A., 2020. Crosslinking strategies for 3D bioprinting of polymeric hydrogels. *Small*, *16*(35), p.2002931.

[48] Bruchet, M. and Melman, A., 2015. Fabrication of patterned calcium cross-linked alginate hydrogel films and coatings through reductive cation exchange. *Carbohydrate polymers*, *131*, pp.57-64.

[49] Bertassoni, L.E., Cardoso, J.C., Manoharan, V., Cristino, A.L., Bhise, N.S., Araujo, W.A., Zorlutuna, P., Vrana, N.E., Ghaemmaghami, A.M., Dokmeci, M.R. and Khademhosseini, A., 2014. Direct-write bioprinting of cell-laden methacrylated gelatin hydrogels. *Biofabrication*, *6*(2), p.024105.

[50] Kolesky, D.B., Truby, R.L., Gladman, A.S., Busbee, T.A., Homan, K.A. and Lewis, J.A., 2014. 3D bioprinting of vascularized, heterogeneous cell-laden tissue constructs. *Advanced materials*, *26*(19), pp.3124-3130.

[51] Ma, Y., Ji, Y., Huang, G., Ling, K., Zhang, X. and Xu, F., 2015. Bioprinting 3D cell-laden hydrogel microarray for screening human periodontal ligament stem cell response to extracellular matrix. *Biofabrication*, *7*(4), p.044105.

[52] Boularaoui, S., Al Hussein, G., Khan, K.A., Christoforou, N. and Stefanini, C., 2020. An overview of extrusion-based bioprinting with a focus on induced shear stress and its effect on cell viability. Bioprinting, p.e00093.

[53] Raveendran, N.T., Vaquette, C., Meinert, C., Ipe, D.S. and Ivanovski, S., 2019. Optimization of 3D bioprinting of periodontal ligament cells. Dental Materials, 35(12), pp.1683-1694.

[54] Ning, L., Betancourt, N., Schreyer, D.J. and Chen, X., 2018. Characterization of cell damage and proliferative ability during and after bioprinting. ACS Biomaterials Science & Engineering, 4(11), pp.3906-3918.

[55] Reid, J.A., Mollica, P.A., Johnson, G.D., Ogle, R.C., Bruno, R.D. and Sachs, P.C., 2016. Accessible bioprinting: adaptation of a low-cost 3D-printer for precise cell placement and stem cell differentiation. Biofabrication, 8(2), p.025017.

[56] Ouyang, L., Yao, R., Mao, S., Chen, X., Na, J. and Sun, W., 2015. Three-dimensional bioprinting of embryonic stem cells directs highly uniform embryoid body formation. Biofabrication, 7(4), p.044101.

[57] Caffall, K.H. and Mohnen, D., 2009. The structure, function, and biosynthesis of plant cell wall pectic polysaccharides. *Carbohydrate research*, *344*(14), pp.1879-1900.

[58] Thakare, K., Wei, X., Jerpseth, L., Bhardwaj, A., Qin, H. and Pei, Z., 2020. Feasible regions of bioink composition, extrusion pressure, and needle size for continuous extrusion-based bioprinting. *Journal of Manufacturing Science and Engineering*, *142*(12), p.124501.

[59] Lim, K.S., Schon, B.S., Mekhileri, N.V., Brown, G.C., Chia, C.M., Prabakar, S., Hooper, G.J. and Woodfield, T.B., 2016. New visible-light photoinitiating system for improved print fidelity in gelatin-based bioinks. *ACS biomaterials science & engineering*, *2*(10), pp.1752-1762.

[60] Zhuang, P., Ng, W.L., An, J., Chua, C.K. and Tan, L.P., 2019. Layer-by-layer ultraviolet assisted extrusion-based (UAE) bioprinting of hydrogel constructs with high aspect ratio for soft tissue engineering applications. *PLoS One*, *14*(6), p.e0216776.

[61] Trachtenberg, J.E., Placone, J.K., Smith, B.T., Piard, C.M., Santoro, M., Scott, D.W., Fisher, J.P. and Mikos, A.G., 2016. Extrusion-based 3D printing of poly (propylene fumarate) in a full-factorial design. *ACS Biomaterials Science & Engineering*, *2*(10), pp.1771-1780.